

# The distribution of annihilation luminosities in dark matter substructure

Savvas M. Koushiappas,<sup>1</sup> Andrew R. Zentner,<sup>2</sup> and Andrey V. Kravtsov<sup>3,4,5</sup>

<sup>1</sup>*Department of Physics, Brown University, 182 Hope Street, Providence, RI 02912\**

<sup>2</sup>*Department of Physics & Astronomy, University of Pittsburgh, Pittsburgh, PA 15260†*

<sup>3</sup>*Kaoli Institute for Cosmological Physics, The University of Chicago, Chicago, IL 60637*

<sup>4</sup>*Enrico Fermi Institute, The University of Chicago, Chicago, IL 60637*

<sup>5</sup>*Department of Astronomy & Astrophysics, The University of Chicago, Chicago, IL 60605‡*

We calculate the probability distribution function (PDF) of the expected annihilation luminosities of dark matter subhalos as a function of subhalo mass and distance from the Galactic center using a semi-analytical model of halo evolution. We find that the PDF of luminosities is relatively broad, exhibiting a spread of as much as an order of magnitude at fixed subhalo mass and halo-centric distance. The luminosity PDF allows for simple construction of mock samples of  $\gamma$ -ray luminous subhalos and assessment of the variance in among predicted  $\gamma$ -ray signals from dark matter annihilation. Other applications include quantifying the variance among the expected luminosities of dwarf spheroidal galaxies, assessing the level at which dark matter annihilation can be a contaminant in the expected  $\gamma$ -ray signal from other astrophysical sources, as well as estimating the level at which nearby subhalos can contribute to the antimatter flux.

PACS numbers: 95.35.+d, 98.35.Gi, 98.35.Pr, 98.62.Gq

## I. INTRODUCTION

Multiple lines of observational evidence have established the existence of a form of non-baryonic dark matter binding galaxies. Dark matter is commonly considered a yet-to-be discovered elementary particle. A promising candidate is a Weakly-Interacting Massive Particle (WIMP) that arises in extensions to the standard model of particle physics. Examples include the lightest supersymmetric particle [1, 2] and particle excitations in theories of Universal Extra Dimensions [3]. WIMPs interact via the Weak interaction and were in thermal equilibrium in the early Universe. If the dark matter is a thermal relic WIMP, the WIMP annihilation cross section can be constrained by requiring that the present dark matter density is  $\Omega_c \approx 0.23$  [4]. Implied values for this cross section are of order  $\langle\sigma v\rangle \sim 10^{-26} \text{ cm}^3/\text{s}$ , and candidate WIMPs can annihilate to many observable states, such as  $\gamma$ -rays and high-energy neutrinos.

The Cold Dark Matter (CDM) model of cosmological structure formation predicts that dark matter is distributed in “halos” in a hierarchical fashion. The host halo of the Milky Way is expected to have mass of  $M \approx 10^{12} h^{-1} M_\odot$  [5, 6]. Within the CDM model such halos are also expected to contain numerous smaller dark matter “subhalos” which, in turn, contain subhalos of their own, perhaps with masses all the way down to the cutoff scale in the primordial density fluctuation power spectrum [7–10].

A well-studied avenue for possible identification of the dark matter is to search for unique products of dark

matter annihilation at the center of our Galactic halo, where densities are highest [11–18]. However, astrophysical backgrounds are also highest toward the Galactic center, so an alternative approach is to search for annihilation within subhalos [19–31] (including potentially sub-solar mass halos [30, 32–36]), or to infer annihilation within subhalos statistically through the angular distribution of diffuse  $\gamma$ -ray emission [37–47]. More recently, the one-point  $\gamma$ -ray flux probability distribution function (PDF) was proposed as another way to quantify the expected annihilation signal [43]. The main idea behind this approach is that the pixel-to-pixel flux variation from  $\gamma$ -ray emission from small dark matter subhalos would deviate from the Poisson fluctuations that would be expected from a smoothly-distributed dark matter halo and smoothly-distributed backgrounds.

A calculation of the contribution of annihilation products from subhalos to the flux along any sight line consists of the following two ingredients. The first is the number of subhalos intercepted along the line of sight, assuming subhalos to be small compared to the angular resolution of the instrument as is the case with contemporary detectors. The second is the annihilation luminosity of each intercepted subhalo. The latter depends on the distribution of dark matter within subhalos, which reflects the underlying process of nonlinear mass assembly individual to each subhalo. Although two subhalos may have the same mass and be located at the same Galactocentric distance today, they may have different annihilation luminosities because they may have different formation times, mass assembly histories, and different orbits in the Milky Way potential. Each of these factors affects the internal densities of subhalos. Therefore, we expect a distribution of luminosities at each subhalo mass and Galactocentric distance.

In this paper, we estimate the probability distribution function (PDF) of the subhalo luminosity as a function

\*Electronic address: koushiappas@brown.edu

†Electronic address: zentner@pitt.edu

‡Electronic address: andrey@oddjob.uchicago.edu

of the subhalo mass and Galacto-centric distance from a large ensemble of subhalo populations generated using a semi-analytic model of halo and subhalo evolution [48]. Our aim is to use a statistically-large sample of subhalo properties to provide a useful tool for computing subhalo annihilation signals in a way that captures some of the complexity of nonlinear evolution. We show that the luminosity PDF of subhalos is well fit by a log-normal distribution, reflecting the underlying distribution in formation times (or concentrations, [49, 50]) and provide simple, empirical fits to the luminosity PDFs as a function of mass and distance. Applications for the derived PDF range from quantifying the variance in the expected luminosities of dwarf spheroidal galaxies to generating mock synthetic  $\gamma$ -ray sky maps, to understanding the level at which dark matter annihilation can be a contaminant in the expected  $\gamma$ -ray signal from other astrophysical sources [51–54], and to ascertain the level at which a nearby subhalo can contribute to the measured flux of antimatter [55].

## II. THE IMPORTANCE OF THE SUBHALO LUMINOSITY PDF

The effects of a distribution of luminosities on any calculation that involves the diffuse emission is only important if most of the diffuse flux originates from a large number of sources. If, for example, the diffuse flux is due to very few sources with high luminosities, then the properties of the diffuse background would be dominated by the Poisson statistics of the emission of photons from these sources. If, on the other hand, there are many dim sources along the line of sight, the intrinsic variation in the luminosities of these sources will have an effect on the flux PDF. This is due to the fact that the flux PDF will deviate from Poisson statistics as it will depend not only on the flux-density distribution but also on the mean number of sources (see the ‘ $P(D)$  analysis’ discussion in the Appendix of Lee et al. [43]).

We can quantify this argument as follows. Suppose the number density of subhalos of luminosity  $L$  at position  $\ell$  along a particular line of sight is given by  $dN/dM dV \propto M^{-\alpha} n[\ell(r)]$ , where  $n[\ell(r)]$  is the number density of subhalos at Galacto-centric distance  $r$  along line of sight distance  $\ell$ . Additionally, assume a mapping between the luminosity and the mass of a subhalo,  $L \propto M^\beta$ . Then the contribution to the received flux that is produced by subhalos in a given logarithmic mass and line of sight interval is given by

$$\tilde{F}_{M,\ell} \equiv \frac{dF}{d \ln M d \ln \ell} \propto M^{-\alpha+\beta+1} \ell n[r(\ell)], \quad (1)$$

Taking  $\alpha \approx 1.9$  and  $\beta \approx 0.8$  (consistent with analytical arguments [29], and numerical simulations [26, 30, 56]), the flux per logarithmic interval in mass and line of sight distance has a weak dependence on mass  $\tilde{F}_{M,\ell} \propto M^{-0.1}$ .

In order for the low mass subhalo contribution to the annihilation flux to be roughly the same as high mass halos, their abundance must be larger. The mean number of subhalos per logarithmic line of sight interval and logarithmic mass interval is

$$\tilde{N}_{M,\ell} \equiv \frac{dN}{d \ln M d \ln \ell} \propto M^{-\alpha+1} \ell^3 n[r(\ell)]. \quad (2)$$

Assuming that the distribution of subhalos traces that of dark matter,  $n[\tilde{r}(\ell)] \propto [\tilde{r}(1 + \tilde{r})]^{-1}$  [57, 58], where  $\tilde{r} = r/r_s$  and  $r_s$  is the scale radius of the NFW dark matter profile. For  $\alpha \approx 1.9$  and small distances ( $\ell \ll r \ll r_s$ ),  $n[\tilde{r}(\ell)] \propto 1/\tilde{r}(\ell)$  so that  $\tilde{N}_{M,\ell} \propto M^{-0.9} \ell^2$ . For large distances ( $\ell \approx r \gg r_s$ ),  $n[\tilde{r}(\ell)] \propto 1/\tilde{r}^3(\ell)$  and  $\tilde{N}_{M,\ell} \propto M^{-0.9}$ , roughly independent of  $\ell$  for all masses.

The previous two paragraphs show that we should expect the majority of the diffuse annihilation flux to be due to the presence of numerous low-mass subhalos. In the left panel of Fig. 1 we show the quantity  $\tilde{F}_{M,\ell}$  in units of  $\text{cm}^{-2} \text{s}^{-1} \text{sr}^{-1}$ , as a function of subhalo mass and position along the line of sight, Eq. (1), at an angle  $\psi = 90^\circ$  with respect to the Galactic center. We assume a Milky Way halo with a radius  $R_{MW} = 250 \text{ kpc}$ , and a scale radius  $r_s \approx 20 \text{ kpc}$ . Note that at any fixed mass, most of the flux comes from a region at  $\ell \approx 10 \text{ kpc}$ . This is because the number of objects declines rapidly with distance at Galacto-centric distances significantly larger than a scale radius. Moreover, low-mass subhalos contribute marginally more flux than their high-mass counterparts. In the right panel of Fig. 1 we show the mean number per logarithmic mass and line-of-sight interval,  $\tilde{N}_{M,\ell}$ . The two panels of Fig. 1 illustrate a basic conclusion that the mean number of objects along a line of sight increases with decreasing subhalo mass (right panel), and as all intervals of subhalo mass have comparable flux contributions (left panel), the signal is set by relatively low-mass subhalos that are close to the observer. This is in qualitative agreement with the result of Lee et al. [43] who found that substructures give rise to photon counts that deviate from a Poisson distribution.

Our simple demonstration neglects the presence of a baryonic disk in the Milky Way halo, and its effect on the subhalo population in the inner regions of the halo. Recent studies find that the inner 30 kpc of a Milky Way-sized halo may be deficient in subhalos due to interactions with the disk [59]. This should have an effect on the flux contributions we derived, but the approximate mass and distance dependence that we describe should be maintained. Nevertheless, it is important to keep in mind that a depleted subhalo population in the inner regions of the Galactic disk may have an effect on the flux from substructure. The maximal net suppression in annihilation flux near the disk due to this suppression is expected to be a factor of a few [59].

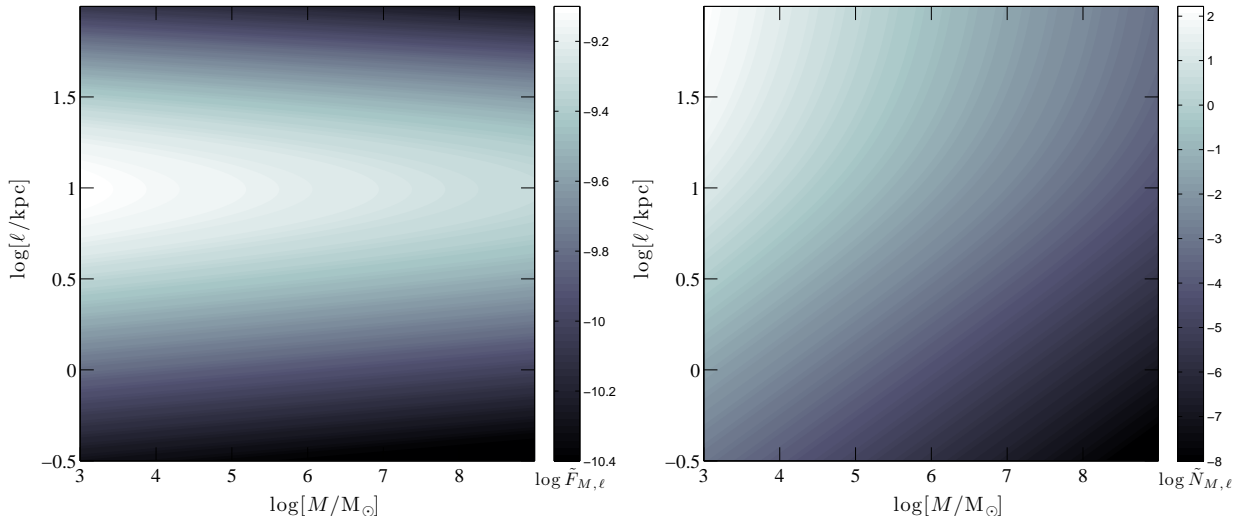


FIG. 1: *Left:* The mean contribution to the annihilation flux from all subhalos in a logarithmic interval of subhalo mass (horizontal axis) and line-of-sight distance (vertical axis),  $\tilde{F}_{M,\ell}$  defined in Eq. (1) in units of  $\text{cm}^{-2}\text{s}^{-1}\text{sr}^{-1}$ . This panel shows the mean contributions along a line of sight  $90^\circ$  away from the Galactic center. The color at each position designates the value of  $\tilde{F}_{M,\ell}$ , where lighter colors indicate larger values as shown in the color bar. The contribution along the line of sight peaks at  $\sim 10$  kpc at all masses. *Right:* The mean number of subhalos per logarithmic interval of subhalo mass and logarithmic line-of-sight interval. Lighter colors designate larger numbers of subhalos according to the color bar. Smaller objects dominate the number density at all radii [see Eq. (2)].

### III. THE SUBHALO ANNIHILATION LUMINOSITY PDF

In order to derive the subhalo luminosity PDF, we model the accretion and dynamical evolution of subhalos in the Milky Way potential well using an approximate semi-analytic technique [48]. This approximate approach greatly reduces the computational cost of modeling substructure by treating subhalo density profiles as continuously-evolving functions that can be described by a small number of parameters, rather than a collection of a very large number of individual particles. This enables calculations of the properties of subhalo populations in a large set of Milky Way-sized halos, so that object-to-object variance can be estimated. This is not yet feasible in simulations directly. This procedure also provides a physically-motivated method to extrapolate the results of numerical simulations to masses below their resolution limits, masses which are not negligible from the annihilation perspective. Of course, the cost of this method is that it is approximate and the approximations implemented cannot be validated outside the range of scales that are resolved by  $N$ -body simulations. This method is described in detail in [48], which also shows a number of non-trivial comparisons with  $N$ -body simulations that validate this treatment of halo substructure.

We use an ensemble of 200 realizations of subhalo populations within a dark matter halo of mass  $M_{\text{MW}} = 1.26 \times 10^{12} h^{-1} M_\odot$  in a flat cosmological model with  $\Omega_{dm} = 0.228$ ,  $\Omega_b h^2 = 0.0227$ ,  $h = 0.71$ , and  $\sigma_8 = 0.81$ , favored by the five-year Wilkinson Microwave Anisotropy

Probe results [4]. Each realization represents a possible subhalo population within a Milky Way-like halo. The populations differ because only some statistical properties of the initial density field in the local neighborhood are known, not the precise initial conditions for collapse. We use this large number of distinct populations to quantify the predicted variation from one Milky Way-sized halo to another. The result of the calculation is a list of all subhalos, complete with their structural parameters such as bound mass, scale radius, and tidal radius. These quantities all evolve with time, and we study them at the present epoch ( $z = 0$ ).

Figure 2 shows the cumulative velocity function of Galactic subhalos. The power-law behavior is similar to what is found in numerical simulations, with the number of subhalos increasing as  $N(> V_{\text{max}}) \propto V_{\text{max}}^{-3}$ . Our model also reproduces the abundance of subhalos in cosmological simulations reasonably well (see also Ref. [48] for a discussion). For example, the average number of subhalos with  $v_{\text{max}} > 4$  km/s within the inner 200 kpc of the Milky Way in our models is 2481 with a 68 percentile range of [1964-3007]. This is consistent with 2469 subhalos of  $v_{\text{max}} > 4$  km/s within the same radius in the Via Lactea II simulation of a Milky Way-sized halo [60]. Moreover, the dispersion in the number of subhalos is consistent with the empirical finding of a Poisson scatter added in quadrature to an intrinsic scatter of about 20% derived from recent numerical simulations [61]. We note that the validation exercises in Ref. [48] show that this model may over-estimate halo-to-halo variance mildly (see their Fig. 7), though it is difficult to assess through a compari-

son with simulations with greater precision at this point.

Note that in general, the slope and normalization of the velocity function depend on the concentration of the host dark matter halo [48]. As shown in Fig. 2, the normalization of the velocity function of subhalos is reduced. This is to be expected as host dark matter halos with high concentrations are formed earlier than low mass halos. As a result, there is more available time for evolution of the subhalo population leading to a decrease in the total number of subhalos. A subsidiary effect that also contributes to the decrease of the subhalo population of high-concentration halos is the efficient tidal disruption due to the higher central densities. On the other hand, subhalos in host halos with low concentrations will, on average, have spent less time in the host and have a higher rate of survival due to the decreased tidal forces.

We model the final dark matter distribution in a subhalo of mass  $M$  as a Navarro-Frenk-White (NFW) profile [57, 58],

$$\rho(r) = \frac{M}{4\pi r_s^3} \frac{1}{f(\tilde{r}_t)} \frac{1}{\tilde{r}(1+\tilde{r})^2}. \quad (3)$$

In Eq. (3),  $\tilde{r} = r/r_s$ , where  $r_s$  is the evolved scale radius.  $f(x) = \ln(1+x) - x/(1+x)$ , and  $\tilde{r}_t = r_t/r_s$  is the ratio of a tidal truncation radius  $r_t$ , to the scale radius. We treat tidal truncation by assuming an abrupt limit to the extent of the subhalo density profile for simplicity. Isolated high-resolution simulations of subhalo evolution support a very sharp truncation (e.g., Ref. [62, 63]) and, furthermore, the annihilation luminosity emanating from the transition region should be very small in comparison to the total annihilation luminosity. Our simplifying assumption of a truncated NFW profile is not crucial to our analysis. Deviations in the assumed power law in the inner regions of the profile do not result in large changes in the total luminosity of the halo. Profiles with different inner slopes also require different normalizations to maintain the same bound mass against the tidal forces of the host. Moreover, much of the total luminosity of a nearly-NFW halo arises from the region near the scale radius,  $r_s$ . As such, changes in the inner slope do not lead to large changes in the annihilation luminosity in most circumstances (see Refs. [23, 27, 29, 64, 65]).

The dark matter luminosity of a subhalo is then obtained from

$$\begin{aligned} L &= 4\pi \frac{\langle\sigma v\rangle N_\gamma^{\text{tot}}}{M_\chi^2} \int_0^{r_t} \rho^2 r^2 dr \\ &= \frac{3.32 \times 10^{37} \text{ ph}}{\text{s}} \frac{\langle\sigma v\rangle_{-26} N_{\gamma,30}^{\text{tot}}}{M_{\chi,100}^2} \\ &\quad \times \left(\frac{r_s}{\text{kpc}}\right)^3 \int_0^{\tilde{r}_t} \left(\frac{\rho(\tilde{r})}{\text{GeV/cm}^3}\right)^2 \tilde{r}^2 d\tilde{r}. \end{aligned} \quad (4)$$

Here,  $\langle\sigma v\rangle_{-26}$  is the annihilation cross section in units of  $3 \times 10^{-26} \text{ cm}^3 \text{ s}^{-1}$ ,  $M_{\chi,100}$  is the mass of the dark matter particle in units of 100 GeV, and  $N_{\gamma,30}^{\text{tot}}$  is the total number of photons emitted above a threshold of 1 GeV, in

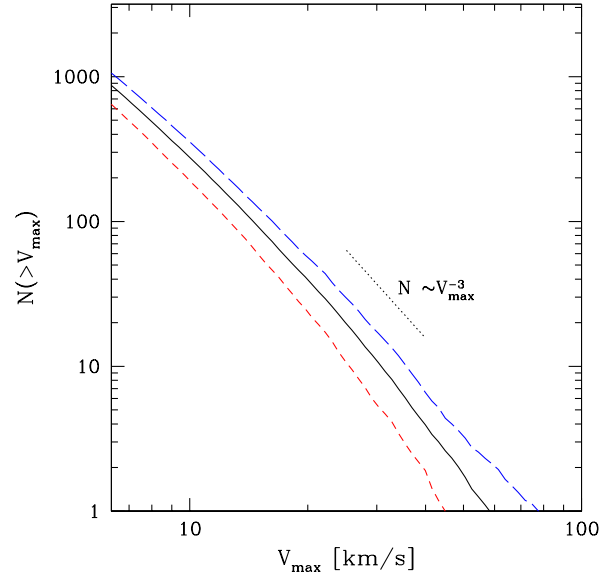


FIG. 2: The cumulative velocity function of subhalos. The solid black line shows the average velocity function over all 200 realizations of the formation of a Milky Way-size halo. The short-dashed red line shows the velocity function derived for Galactic halos which have a concentration  $c > 13.4$ , while the long-dashed blue line shows the velocity function for Galactic halos with  $c < 6.7$ . The dotted line shows the behavior of a  $N(> V_{\text{max}}) \propto V_{\text{max}}^{-3}$  power law, which describes the subhalo velocity function in cosmological simulations.

units of 30. This fiducial choice of parameters is representative of optimistic scenarios in the Minimal Supersymmetric Model. We emphasize that we defined luminosity as *number of photons per unit time*, and not energy per time. Similarly, when we discuss flux, we implicitly mean photon flux, and not the energy flux. Note also that as the goal of this work is to quantify the spread in luminosities in the subhalo population, the choice of particle physics parameters in Eq. 4 is intended only to provide a useful representation of the magnitude of the luminosity. However, the PDFs of luminosities derived below are affected by the choice of particle physics parameters only in their normalization.

## IV. RESULTS

We compute subhalo luminosities as a function of radial position and mass as follows. We first determine the minimum and maximum of the radial distribution (typically  $r_{\text{min}} \sim \text{kpc}$ ,  $r_{\text{max}} \sim 250 \text{ kpc}$ ) of subhalos as well as the minimum and maximum subhalo mass at the present epoch (typically  $M_{\text{min}} \sim 10^4 M_\odot$ ,  $M_{\text{max}} \sim 10^{11} M_\odot$ ). We then divide the radial distribution of subhalos into  $N_r$  bins. Each radial bin is then subdivided into  $N_m$  mass bins of equal logarithmic size in mass. We then fit the *distribution* of luminosities for different values of  $N_r$

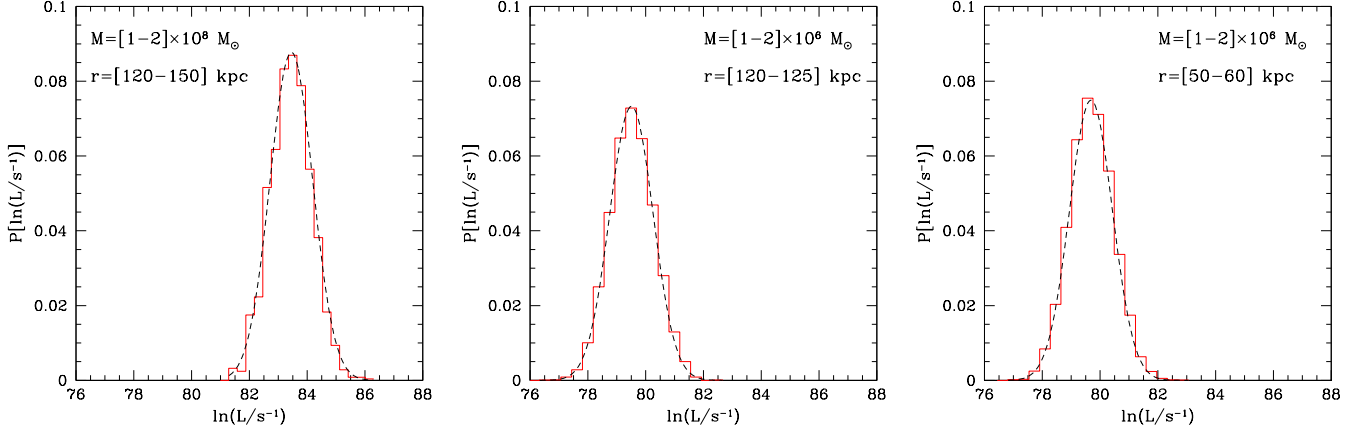


FIG. 3: Example probability distribution functions of the  $\gamma$ -ray luminosity for three sample mass and radial bins. The solid curve depicts a histogram of the distribution of luminosities in each bin. The dashed curve shows the fitting function of Eq. 5.

and  $N_m$  until the maximum deviation of the fit is less than 10% of the true value. We find that  $N_m = N_r = 50$  with at least 200 subhalos per bin has errors of at most 10% of the true value.

The luminosity of a subhalo is a function of its mass as well as its position within the host halo. We find that the subhalo luminosity PDF is well fit by a log-normal distribution, as

$$P[\ln L_{M,r}] = \frac{1}{\sqrt{2\pi}} \frac{1}{\sigma_{M,r}} \exp \left[ -\frac{[\ln L_{M,r} - \langle \ln L_{M,r} \rangle]^2}{2\sigma_{M,r}^2} \right] \quad (5)$$

where,

$$\langle \ln L_{M,r} \rangle = a_1 + a_2 \ln \left( \frac{M}{10^5 M_\odot} \right) + a_3 \ln \left( \frac{r}{50 \text{ kpc}} \right), \quad (6)$$

and,

$$\sigma_{M,r} = b_1 + b_2 \ln \left( \frac{M}{10^5 M_\odot} \right) + b_3 \ln \left( \frac{r}{50 \text{ kpc}} \right). \quad (7)$$

Here, we implicitly assume that the luminosity  $L_{M,r}$  is expressed in units of photons per second.

Assuming the fiducial particle physics parameters as shown in Eq. 4, the best fit parameters for the whole population of subhalos in all 200 realizations are  $a_1 = 77.5$ ,  $a_2 = 0.87$ ,  $a_3 = -0.22$ ,  $b_1 = 0.75$ ,  $b_2 = -0.0026$ , and  $b_3 = 0.0061$  (see “All” in Table I). This result can be scaled to any assumed particle physics parameters, by simply adding the term

$$\ln \left( \frac{N_\gamma^{\text{tot}} \langle \sigma v \rangle M_\chi^{-2}}{9 \times 10^{-29} \text{ cm}^3 \text{ s}^{-1} \text{ GeV}^{-2}} \right) \quad (8)$$

to the parameter  $a_1$  of Eq. 6

The fitting function [Eq. 5 with Eq. (6) & Eq. (7)] is good to within  $\sim$  a few % for  $P[\ln L_{M,r}]$  as a function of  $\ln L_{M,r}$  over the range of masses and radii we have examined with sufficient statistics,  $M \approx [10^4 - 10^{10}] M_\odot$ , and

	$a_1$	$a_2$	$a_3$	$b_1$	$b_2$	$b_3$
All	77.4	0.87	-0.22	0.75	-0.0026	0.0061
$C_0$	77.4	0.87	-0.23	0.74	-0.0030	0.011
$C_+$	77.5	0.87	-0.26	0.76	-0.0021	0.0077
$C_-$	77.3	0.87	-0.18	0.75	-0.0013	0.0043

TABLE I: Fitting parameters for the mean and width of the  $\gamma$ -ray annihilation flux distribution function (see text).

$r \approx [5 - 250] \text{ kpc}$ . The mean and variance of the distribution are functions of mass and radius, reflecting the fact that the PDF of luminosity is set by the interplay between the mass function of accreted objects, the redshift of accretion, and the orbital evolution of the individual subhalos constituting the population.

The mean luminosity of isolated, field halos that have *not* experienced strong interactions within the potential of a more massive halo, scales as  $L \propto \rho_s^2 r_s^3 \propto M c^3 / f^2(c)$ , where  $M$  is the halo mass, corresponding to a virial radius  $R \propto M^{1/3}$ ,  $c \equiv R/r_s$  is the concentration and  $f(c) \propto c^{0.4}$  near  $c \approx 30$  as is relevant for small subhalos [27]. If we assume a weak dependence of concentration on mass  $c(M) \propto M^{-0.1}$  [49, 50, 66–68], the luminosity of a halo scales roughly as  $L \propto M^{0.8}$ . However, subhalo populations deviate from this scaling somewhat for several reasons. Subhalos merge into the host halo at a variety of times, so they sample the  $c(M)$  relation at a variety of redshifts and subhalos of fixed mass at the time of merger exhibit a variety of bound masses at  $z = 0$  as a result of their distinct orbital evolution histories. Therefore, subhalo luminosities at fixed mass are influenced by the mass and redshift dependence of concentrations and subhalo orbital properties. The effects of these physical changes in the structure and description of subhalos compared to isolated halos are reflected in the best fit parameters of Eq. 6. In particular, we find that the luminosity of *evolved* subhalos scales approximately as  $L \propto M^{0.87}$ .

In Figure 3 we show the distribution of luminosities

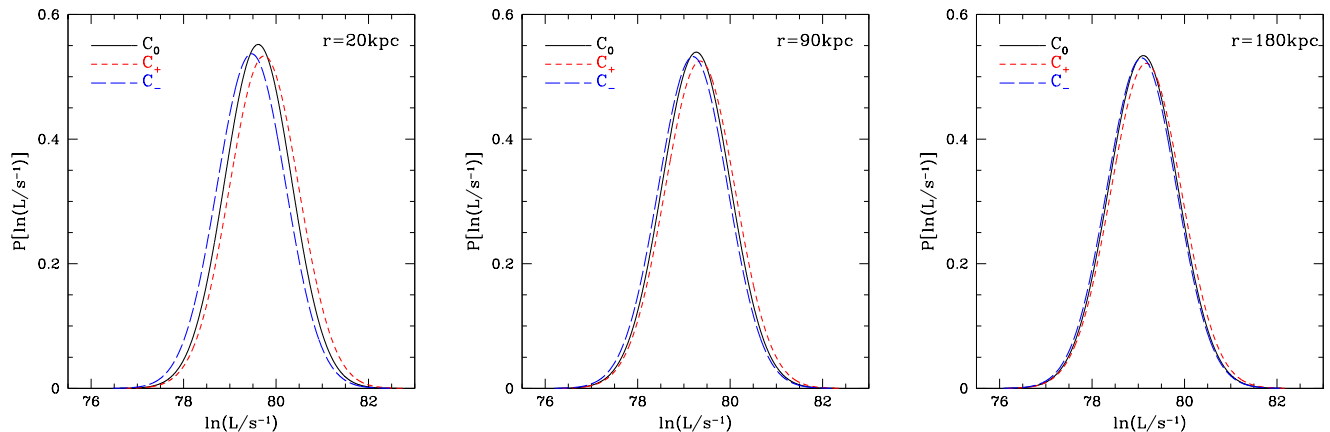


FIG. 4: Probability distribution functions of the  $\gamma$ -ray luminosity of a  $10^6 M_\odot$  subhalo at three different radial distances from the Galactic center (Eq. 5 and parameters from Table I). The solid curve depicts a histogram of the distribution of luminosities in host halos with a concentration in the 68 percentile about the mean of the sample of 200 realizations ( $C_0$ ). The short-dashed curve shows the subhalo luminosity PDF for host halos with a concentration in the upper 16 percent ( $C_+$ ), while the long-dashed curve shows the subhalo luminosity PDF for host halos with a concentration in the lower 16 percent ( $C_-$ ).

in three examples of radial and mass bins. The figure also shows the fit to the luminosity distribution given in Eq. (5). The choice of mass and radius displayed in Fig. 3 are only meant to demonstrate schematically the agreement between the fitting functions and the numerical results. Notice that the spread in luminosities at fixed mass and position can be roughly *an order of magnitude*, and that the peak of the luminosity PDF depends on both, mass as well as radius.

As the structural properties and abundances of subhalos are influenced by the merger history and properties of the host halo, we expect that the luminosity PDF will be affected by the distribution of dark matter within the host dark matter halo. In order to explore the relationship between the host halo properties and the subhalo luminosity PDF we divided the subhalo populations into three groups based upon the concentrations of their host halos. We grouped subhalos with host halo concentrations within the 68% range of the mean concentration,  $\bar{c} = 9.7$ . This group, “ $C_0$ ”, consists of subhalos in primaries with concentrations in the range  $6.7 \leq c \leq 13.4$ . We then collected all subhalos in hosts in the upper and lower 16% ranges, with group  $C_-$  consisting of host concentrations in the range  $c < 6.7$  and group  $C_+$  consisting of primaries with  $c > 13.4$ . The fitting parameters of Eq. (5) for these three concentration bins are also given in Table I.

Fig. 4 shows the effects of the host halo concentration on the luminosity PDF of subhalos. At inner radii (left panel of Fig. 4), the effects are more pronounced. This is the region where earliest merging subhalos reside. Host halos with high concentrations are formed early, and contain subhalos that on average have formed earlier, and so are also more concentrated [50]. As the annihilation signal is sensitive to the concentration of subhalos [27], the luminosity of subhalos in a high concentration host

is slightly higher ( $C_+$  curve in Fig. 4) than subhalos residing in host halos with lower concentration ( $C_-$  curve in Fig. 4). At large radii,  $r > r_s$  (right panel of Fig. 4) the difference between host halos of different concentrations diminishes, reflecting the fact that the outer regions of halos typically contain recently-merged substructure (the host concentration influences subhalo dynamics little beyond the halo scale radius). Fig. 4 and Table I demonstrate that the maximum shift in typical subhalo luminosities is in the inner regions of host halos, and is relatively small,  $\sim 20\%$ .

## V. APPLICATIONS

The flux PDFs that we provide have numerous potential applications. As an example, in this section we compute the probability distribution for measuring a flux between  $F$  and  $F + dF$  from *any individual subhalo* along a line of sight at an angle  $\psi$ , from the Galactic center. We compute this “single halo flux PDF” as

$$P_1[F|\psi] \propto \int_0^{\ell_{\max}} \int_{M_{\min}}^{M_{\max}} \ell^4 \frac{dN[r(\ell, \psi)]}{dM dV} \times P[L_{F,\ell}|M, r(\ell, \psi)] dM d\ell \quad (9)$$

Here,  $\ell$  is the line-of-sight distance,  $dN[r(\ell, \psi)]/dM dV$  is the subhalo mass function, and  $L_{F,\ell} = 4\pi\ell^2 F$  ensures a proper flux measurement for a subhalo of luminosity  $L$  at a distance  $\ell$ . The quantity  $\ell_{\max}$  is the maximum line-of-sight distance we consider, given by

$$\ell_{\max} = d_\odot \left[ \cos \psi + \sqrt{(R_G/d_\odot)^2 - \sin^2 \psi} \right], \quad (10)$$

where  $d_\odot = 8 \text{ kpc}$  is the distance of the Sun to the Galactic center, and  $R_G = 250 \text{ kpc}$  is the approximate radius



of the Galactic halo. As in Sec. II, we assume a mass function of the form  $dN/dM dV \propto M^{-\alpha}/\tilde{r}(1+\tilde{r})$ , with  $\alpha = 1.9$ , as predicted by both N-body simulations [69], as well as by the semi-analytic model of subhalo populations we use for this study. Both simulations and our analytic method show little evidence that  $\alpha$  varies significantly as a function of radius [30, 48, 69], so any variations are subtle (though they may depend upon global host halo properties). Consequently, it is convenient and informative to couple standard halo mass functions with our luminosity PDFs to estimate relevant observable quantities. However, we emphasize that this particular choice of mass function is not unique and, in principle, the flux PDF can be derived using Eq. (5) with a variant subhalo mass function.

In Figure 5 we show the normalized single halo flux probability distribution function for two different lines of sight generated from the contributions of subhalos in the range  $M_{\min} = [10^4 - 10^{10}]M_{\odot}$  (thick lines) and  $M_{\min} = [10^5 - 10^{10}]M_{\odot}$  (thin lines). This choice of subhalo mass does not affect the overall shape of the mass function. A change in the value of  $M_{\max}$  does not affect the result as the mass function power law is a steep decreasing function of mass (see also the left panel of Fig. 1, which shows how the average flux due to high-mass halos is lower than that due to low-mass halos). The high-flux power-law shape of the flux PDF can be understood in the following way. As the mass function is proportional to  $dN/dM dV \propto M^{-1.9}$ , and the luminosity of a subhalo scales with mass as  $L \propto M^{0.87}$  (see Table I), then the integrand is proportional to  $L^{-2.03}$ . However,  $F \propto L/\ell^2$ , so the flux PDF is a power law with a shape given roughly by  $P[F] \propto F^{-2.03}$ . This is apparent for both lines of sight in the high-flux regime.

Changes in the value of  $M_{\min}$  affect the low-flux behavior of the flux PDF. It is easier to understand the low-flux cutoff if we assume a delta function luminosity PDF instead of the log-normal distribution, as in [43]. For a line of sight at some angle  $\psi$ , there is a maximum distance  $\ell_{\max}$  which is a function of  $\psi$  and the radius of the Milky Way halo. If we assume that  $L \propto M$ , and that the subhalo radial distribution is the same for all masses, then the *minimum* flux would be given by  $F_{\min} \propto M_{\min}/\ell_{\max}^2$ , i.e., the smaller the minimum mass, the broader the  $P_1(F)$ . For illustrative purposes we show the  $P_1(F)$  flux PDF derived under the assumption of a delta function luminosity PDF as in [43] in Fig. 5. Assuming the log-normal luminosity PDF (instead of a delta function), results in a tail in the low-flux region of the  $P_1(F)$ , and thus a broader  $P_1(F)$  PDF.

The slope of the flux PDF for low fluxes does depend on the angle between the line of sight and the Galactic center (see the blue solid, and red dashed lines in Fig. 5). At small angles, there is flux probability excess in the low flux regime relative to the high flux region. This can be explained using Fig. 1. At large angles from the Galactic center, the total number of halos intercepted along a line of sight is smaller than the total number of

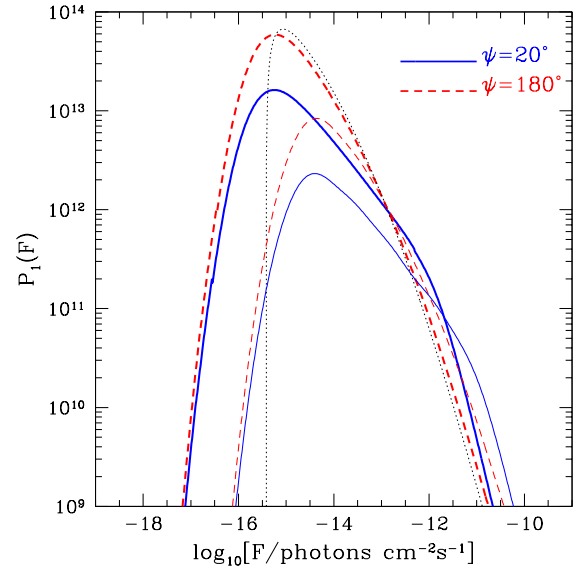


FIG. 5: The flux probability distribution function derived using Eq. 5 and the  $C_0$  parameters of Table I. The solid blue lines is the flux PDF along a line of sight at  $20^\circ$  relative to the Galactic center, while the dashed red lines are along  $180^\circ$ . Thick lines correspond to a minimum subhalo mass of  $10^4 M_{\odot}$ , while thin lines correspond to a minimum subhalo mass of  $10^5 M_{\odot}$ . The black dotted line depicts the single halo flux PDF derived under the assumption of a delta function luminosity PDF.

halos intercepted along a line of sight that passes near the Galactic center. In addition, the fraction of these halos that are close to the Sun is smaller for large  $\psi$ . Therefore, any effects due to the spread of luminosities will be more pronounced where the fraction of contributing sources is large, and also nearby (due to the  $1/\ell^2$  term). The spread of luminosities thus introduces a spread in flux, giving rise to substantial a change in the power-law behavior of the flux PDF.

It is important to draw the distinction between the single halo flux PDF (Eq. 9) and the probability distribution function of measuring a *total* flux  $P(F)$ , from the contribution of numerous halos along the line of sight. The total flux PDF can be computed in a straightforward manner from the basic quantity  $P_1(F)$  [70–74], and more recently [43]). A thorough investigation of the total flux PDF using the single halo PDF  $P_1(F)$ , is presented in [75], where the authors evaluate the ability of FGST to discover dark matter via  $\gamma$ -rays from Galactic substructure.

Another possible application of the luminosity PDF is in the intrinsic spread of the expected  $\gamma$ -ray luminosity signal from dwarf spheroidal galaxies in the Milky Way halo. Dwarf spheroidals are very low surface brightness systems dynamically bound to the dark matter halo of the Milky Way. Their very high mass-to-light ratios make them ideal for  $\gamma$ -ray studies as their dark matter distributions can be well constrained using the ve-

locity dispersions of their stellar populations. Numerous studies addressed the possibility of detecting dark matter annihilation in dwarf spheroidals using either FGST or ground-based Čerenkov telescopes, such as VERITAS and H.E.S.S. [19–23, 31]. Dynamical studies of the velocity dispersion of stars in these systems constrain the dark matter mass (and profile) [29, 31]. Suppose that a group of dwarf spheroidal galaxies have masses estimated via dynamical measurements. The luminosity PDF presented in Sec. IV can be used to assess the expected variance of a possible detection of  $\gamma$ -rays from either Čerenkov telescopes or the FGST. The estimated variance can be used in concert with the measurement of the distribution of dark matter from dynamical studies in the interpretation of any signals or limits from these systems.

Moreover, the use of the luminosity PDF can be important in studies aimed at disentangling the different source contributions to the diffuse gamma-ray background, such as blazars, starburst galaxies, pulsars, supernova remnants, and potentially cataclysmic binary systems, and dark matter [38–42, 46, 47, 51–54, 76]. A useful tool in these studies is the use of the angular correlation function of flux fluctuations, which is estimated from the convolution of the emissivity as a function of distance and the spatial correlation function of the sources. Knowledge of the expected distribution in luminosities of contributing dark matter substructure can be used to remove the dark matter contamination to the astrophysical background, and thus potentially open the window for the detection of  $\gamma$ -rays from yet undiscovered sources [52, 77, 78].

Finally, the annihilation luminosity PDF can be used in studies aimed at estimating the likelihood that nearby dark matter subhalos contribute significantly to the measured antimatter flux [79, 80]. A dark matter explanation for the anomalous excess in antimatter flux must rely on either non-standard extensions to the standard model of particle physics (prominent annihilation to charged leptons [81–84], or some new, long-range force [85], or potentially the presence of a dark matter halo in the near solar-system neighborhood [55]). The luminosity PDF presented in this paper can be used to assess the minimum spread of the expected flux from a given subhalo and the likelihoods of particular flux measurements from rare, nearby objects. Note however, that propagation effects as well as the degeneracy between luminosity and the square of the distance to the subhalo, and velocity-dependent annihilation [65, 86, 87] can all increase the spread considerably.

## VI. CONCLUSIONS

We have presented an estimate of the luminosity probability distribution function of dark matter subhalos

within a Milky Way-like parent halo. An empirical fit to our numerical calculations suggest that the luminosity PDF can be described well by a log-normal distribution with subhalo mass- and position-dependent mean and variance. This log-normal probability distribution has a width that is determined by the wide distribution of formation times and concentrations for both the host halo and subhalos.

The derived luminosity PDF can be used as an ingredient in a number of interesting calculations regarding predictions for observable dark matter annihilation products. This distillation of a complex set of halo properties should be particularly useful with the impending data from the Fermi Gamma-ray Space Telescope and continued advances of ground-based Air Čerenkov Telescopes as well as neutrino telescopes and antimatter detection instruments. The tool we provide can be used to address such observations, including variance in the predicted signal, in a relatively simple manner.

As a straightforward example of the application of the PDF, we have estimated the distribution of observed  $\gamma$ -ray fluxes along lines of sight as a function of the angular separation between the line-of-sight and the Galactic center. This may be used as a signature to diagnose unresolved annihilation in a population of Galactic subhalos (see [75], where the authors utilize this distribution to estimate the robustness of estimating dark matter properties from the diffuse flux measurements of FGST). Additional applications of the annihilation luminosity PDF include estimates in the spread of the angular power spectrum of flux fluctuations as a probe of unresolved substructure in the Milky Way, as well as the antimatter flux distribution from nearby subhalos. These applications make the luminosity PDF a useful tool in the analysis of forthcoming data in the ongoing effort to identify the dark matter.

## Acknowledgments

SMK and AVK thank the Center for Scientific Computation and Mathematical Modeling at the University of Maryland College Park for hospitality. We thank Eric J. Baxter, Scott Dodelson and Louie Strigari for useful comments. ARZ acknowledges the support and hospitality of the Michigan Center for Theoretical Physics at the University of Michigan. SMK is funded by the NSF and by Brown University. ARZ is funded by the University of Pittsburgh, by the NSF through grant AST-0806367, and by the DoE. AVK is supported by the DoE and NSF grant AST-0708154, and by the Kavli Institute for Cosmological Physics at the University of Chicago through the NSF grant PHY-0551142 and an endowment from the Kavli Foundation.



- 
- [1] G. Jungman, M. Kamionkowski, and K. Griest, *Phys. Rept.* **267**, 195 (1996).
  - [2] G. Bertone et al., *Phys. Rept.* **405**, 279 (2005).
  - [3] D. Hooper and S. Profumo, *Phys. Rept.* **453**, 29 (2007), hep-ph/0701197.
  - [4] E. Komatsu et al. (WMAP), *Astrophys. J. Suppl.* **180**, 330 (2009), 0803.0547.
  - [5] A. Klypin, H. Zhao, and R. S. Somerville, *Astrophys. J.* **573**, 597 (2002), astro-ph/0110390.
  - [6] Y.-S. Li and S. D. M. White, *Mon. Not. Roy. Astron. Soc.* **384**, 1459 (2008), 0710.3740.
  - [7] C. Schmid et al., *Phys. Rev.* **D59**, 043517 (1999).
  - [8] A. M. Green, S. Hofmann, and D. J. Schwarz, *Mon. Not. Roy. Astron. Soc.* **353**, L23 (2004).
  - [9] A. M. Green et al., *JCAP* **0508**, 003 (2005).
  - [10] S. Hofmann et al., *Phys. Rev.* **D64**, 083507 (2001).
  - [11] S. Dodelson, D. Hooper, and P. D. Serpico, *Phys. Rev.* **D77**, 063512 (2008), 0711.4621.
  - [12] P. D. Serpico and G. Zaharijas, *Astropart. Phys.* **29**, 380 (2008), 0802.3245.
  - [13] P. Gondolo and J. Silk, *Phys. Rev. Lett.* **83**, 1719 (1999), astro-ph/9906391.
  - [14] D. Horns, *Phys. Lett.* **B607**, 225 (2005), astro-ph/0408192.
  - [15] D. Merritt, M. Milosavljevic, L. Verde, and R. Jimenez, *Phys. Rev. Lett.* **88**, 191301 (2002), astro-ph/0201376.
  - [16] L. Bergstrom, P. Ullio, and J. H. Buckley, *Astropart. Phys.* **9**, 137 (1998), astro-ph/9712318.
  - [17] R. Aloisio, P. Blasi, and A. V. Olinto, *JCAP* **0405**, 007 (2004), astro-ph/0402588.
  - [18] G. Zaharijas and D. Hooper, *Phys. Rev.* **D73**, 103501 (2006), astro-ph/0603540.
  - [19] E. A. Baltz, C. Briot, P. Salati, R. Taillet, and J. Silk, *Phys. Rev.* **D61**, 023514 (2000), astro-ph/9909112.
  - [20] C. Tyler, *Phys. Rev.* **D66**, 023509 (2002), astro-ph/0203242.
  - [21] N. W. Evans, F. Ferrer, and S. Sarkar, *Phys. Rev.* **D69**, 123501 (2004), astro-ph/0311145.
  - [22] S. Profumo, *Phys. Rev.* **D72**, 103521 (2005), astro-ph/0508628.
  - [23] L. Bergstrom and D. Hooper, *Phys. Rev.* **D73**, 063510 (2006), hep-ph/0512317.
  - [24] C. Calcano-Roldan and B. Moore, *Phys. Rev.* **D62**, 123005 (2000), astro-ph/0010056.
  - [25] A. Tasitsiomi and A. V. Olinto, *Phys. Rev.* **D66**, 083006 (2002), astro-ph/0206040.
  - [26] F. Stoehr, S. D. M. White, V. Springel, G. Tormen, and N. Yoshida, *Mon. Not. Roy. Astron. Soc.* **345**, 1313 (2003), astro-ph/0307026.
  - [27] S. M. Koushiappas, A. R. Zentner, and T. P. Walker, *Phys. Rev.* **D69**, 043501 (2004), astro-ph/0309464.
  - [28] E. A. Baltz, J. E. Taylor, and L. L. Wai, *Astrophys. J. Lett.* **659**, L125 (2007), astro-ph/0610731.
  - [29] L. E. Strigari, S. M. Koushiappas, J. S. Bullock, and M. Kaplinghat, *Phys. Rev.* **D75**, 083526 (2007), astro-ph/0611925.
  - [30] J. Diemand, M. Kuhlen, and P. Madau, *Astrophys. J.* **657**, 262 (2007), astro-ph/0611370.
  - [31] L. E. Strigari et al. (2007), 0709.1510.
  - [32] T. Bringmann, *New J. Phys.* **11**, 105027 (2009), 0903.0189.
  - [33] S. M. Koushiappas, *New J. Phys.* **11**, 105012 (2009), 0905.1998.
  - [34] T. Bringmann and S. Hofmann, *JCAP* **0407**, 016 (2007), hep-ph/0612238.
  - [35] L. Pieri et al., *Phys. Rev. Lett.* **95**, 211301 (2005).
  - [36] S. Ando, M. Kamionkowski, S. K. Lee, and S. M. Koushiappas, *Phys. Rev.* **D78**, 101301 (2008), 0809.0886.
  - [37] S. Ando, *Phys. Rev.* **D80**, 023520 (2009), 0903.4685.
  - [38] S. Ando, E. Komatsu, T. Narumoto, and T. Totani, *Phys. Rev.* **D75**, 063519 (2007), astro-ph/0612467.
  - [39] A. Cuoco et al., *JCAP* **0704**, 013 (2007), astro-ph/0612559.
  - [40] A. Cuoco, J. Brandbyge, S. Hannestad, T. Haugboelle, and G. Miele, *Phys. Rev.* **D77**, 123518 (2008), 0710.4136.
  - [41] M. Fornasa, L. Pieri, G. Bertone, and E. Branchini, *Phys. Rev.* **D80**, 023518 (2009), 0901.2921.
  - [42] D. Hooper and P. D. Serpico, *JCAP* **0706**, 013 (2007), astro-ph/0702328.
  - [43] S. K. Lee, S. Ando, and M. Kamionkowski, *JCAP* **0907**, 007 (2009), 0810.1284.
  - [44] J. M. Siegal-Gaskins (2009), 0907.0183.
  - [45] J. M. Siegal-Gaskins and V. Pavlidou, *Phys. Rev. Lett.* **102**, 241301 (2009), 0901.3776.
  - [46] J. M. Siegal-Gaskins, *JCAP* **0810**, 040 (2008), 0807.1328.
  - [47] M. Taoso, S. Ando, G. Bertone, and S. Profumo, *Phys. Rev.* **D79**, 043521 (2009), 0811.4493.
  - [48] A. R. Zentner, A. A. Berlind, J. S. Bullock, A. V. Kravtsov, and R. H. Wechsler, *Astrophys. J.* **624**, 505 (2005), astro-ph/0411586.
  - [49] J. S. Bullock et al., *Mon. Not. Roy. Astron. Soc.* **321**, 559 (2001).
  - [50] R. H. Wechsler, J. S. Bullock, J. R. Primack, A. V. Kravtsov, and A. Dekel, *Astrophys. J.* **568**, 52 (2002), astro-ph/0108151.
  - [51] S. Ando, E. Komatsu, T. Narumoto, and T. Totani, *Mon. Not. Roy. Astron. Soc.* **376**, 1635 (2007), astro-ph/0610155.
  - [52] F. Miniati, S. M. Koushiappas, and T. Di Matteo, *Astrophys. J.* **667**, L1 (2007), astro-ph/0702083.
  - [53] P.-J. Zhang and J. F. Beacom, *Astrophys. J.* **614**, 37 (2004), astro-ph/0401351.
  - [54] V. Pavlidou and B. D. Fields, *Astrophys. J.* **575**, L5 (2002), astro-ph/0207253.
  - [55] D. Hooper, A. Stebbins, and K. M. Zurek, *Phys. Rev.* **D79**, 103513 (2009), 0812.3202.
  - [56] M. Kuhlen, J. Diemand, and P. Madau (2008), 0805.4416.
  - [57] J. F. Navarro, C. S. Frenk, and S. D. M. White, *Astrophys. J.* **462**, 563 (1996), arXiv:astro-ph/9508025.
  - [58] J. F. Navarro, C. S. Frenk, and S. D. M. White, *Astrophys. J.* **490**, 493 (1997), astro-ph/9611107.
  - [59] E. D'Onghia, V. Springel, L. Hernquist, and D. Keres, *Astrophys. J.* **709**, 1138 (2010), 0907.3482.
  - [60] M. Kuhlen, J. Diemand, P. Madau, and M. Zemp, *J. Phys. Conf. Ser.* **125**, 012008 (2008), 0810.3614.
  - [61] M. Boylan-Kolchin, V. Springel, S. D. M. White, and A. Jenkins (2009), 0911.4484.
  - [62] S. Kazantzidis et al., *Astrophys. J.* **608**, 663 (2004), astro-ph/0312194.
  - [63] S. Kazantzidis, A. R. Zentner, A. V. Kravtsov, J. S. Bullock, and V. P. Debattista, *Astrophys. J.* **700**, 1896

- (2009), 0902.1983.
- [64] D. S. Reed and S. M. Koushiappas (2010), in preparation.
  - [65] B. Robertson and A. Zentner, *Phys. Rev.* **D79**, 083525 (2009), 0902.0362.
  - [66] A. F. Neto et al. (2007), 0706.2919.
  - [67] A. V. Maccio' et al., *Mon. Not. Roy. Astron. Soc.* **378**, 55 (2007), astro-ph/0608157.
  - [68] A. Klypin, S. Trujillo-Gomez, and J. Primack (2010), 1002.3660.
  - [69] V. Springel et al., *Mon. Not. Roy. Astron. Soc.* **391**, 1685 (2008), 0809.0898.
  - [70] X. Barcons, *Astrophys. J.* **396**, 460 (1992).
  - [71] P. A. G. Scheuer and M. Ryle, *Proc. Camb. Phil. Soc.* **53**, 764 (1957).
  - [72] X. Barcons and A. C. Fabian, *Mon. Not. R. Astron. Soc.* **243**, 366 (1990).
  - [73] A. Franceschini, *Astrophys. J. Supp.* **86**, 3 (1982).
  - [74] D. Windridge and S. Phillipps, *Mon. Not. R. Astron. Soc.* **319**, 591 (2000).
  - [75] E. J. Baxter, S. Dodelson, S. M. Koushiappas, and L. E. Strigari (2010), 1006.2399.
  - [76] S. Ando and E. Komatsu, *Phys. Rev.* **D73**, 023521 (2006), astro-ph/0512217.
  - [77] A. Pinzke and C. Pfrommer (2010), 1001.5023.
  - [78] V. Pavlidou and B. D. Fields, *Astrophys. J.* **642**, 734 (2006), astro-ph/0611923.
  - [79] O. Adriani et al. (PAMELA), *Nature* **458**, 607 (2009), 0810.4995.
  - [80] M. Boezio et al., *New J. Phys.* **11**, 105023 (2009).
  - [81] I. Cholis, L. Goodenough, D. Hooper, M. Simet, and N. Weiner, *Phys. Rev.* **D80**, 123511 (2009), 0809.1683.
  - [82] K. M. Zurek, *Phys. Rev.* **D79**, 115002 (2009), 0811.4429.
  - [83] P. J. Fox and E. Poppitz, *Phys. Rev.* **D79**, 083528 (2009), 0811.0399.
  - [84] C.-R. Chen and F. Takahashi, *JCAP* **0902**, 004 (2009), 0810.4110.
  - [85] N. Arkani-Hamed, D. P. Finkbeiner, T. R. Slatyer, and N. Weiner, *Phys. Rev.* **D79**, 015014 (2009), 0810.0713.
  - [86] M. Kuhlen, P. Madau, and J. Silk, *Science* **325**, 970 (2009), 0907.0005.
  - [87] J. M. Cline, A. C. Vincent, and W. Xue, *Phys. Rev.* **D81**, 083512 (2010), 1001.5399.